

High-Entropy Alloys as Catalysts for the CO₂ and CO Reduction Reactions—Part II: Experimental Realization

Subramanian Nellaiappan^{†‡}, Nirmal Kumar Katiyar^{§‡}, Ritesh Kumar^{δ‡}, Arko Parui^δ, Kirtiman Deo Malviya^Υ, K. G. Pradeep[‡], Abhishek K. Singh^{δ*}, Sudhanshu Sharma^{†*}, Chandra Sekhar Tiwary^{#*}, Krishanu Biswas^{§*}

[†]*Department of Chemistry, Indian Institute of Technology Gandhinagar, Gandhinagar - 382355, INDIA; Email: ssharma@iitgn.ac.in*

[§]*Department of Materials Science and Engineering, Indian Institute of Technology Kanpur, Kanpur-208016, INDIA; Email: kbiswas@iitk.ac.in*

^δ*Materials Research Center, Indian Institute of Science, Bangalore-560012, INDIA; Email: abhishek@iisc.ac.in*

^Υ*Department of Materials Engineering, Indian Institute of Science, Bangalore-560012, INDIA*

[‡]*Department of Materials Science and Metallurgical Engineering, Indian Institute of Technology Madras, Chennai-600036, INDIA*

[#]*Metallurgical and Materials Engineering, Indian Institute of Technology Kharagpur, Kharagpur-382355, INDIA; Email: Chandra.tiwary@metal.iitkgp.ac.in*

[‡]Authors have contributed equally in this work.

KEYWORDS: High entropy alloy, redox active, nano-catalysis, CO₂ reduction reaction, DFT stimulation, microscopy analyses

ABSTRACT

Conversion of carbon-di-oxide into selective hydrocarbon using stable catalyst remains a holy-grail in catalysis community. The high overpotential, stability, and selectivity in use of a single metal-based catalyst still remain a challenge. In current work, instead of using pure noble metals (Ag, Au, and Pt) as the catalyst, a nanocrystalline high entropy alloy (HEA: AuAgPtPdCu) has been used for conversion of CO₂ into gaseous hydrocarbons. Utilizing an approach of multi-metallic HEA, a Faradaic efficiency of about 100% towards gaseous products is obtained at the lowest applied potential (-0.3 V vs. reversible hydrogen electrode). The reason behind the superior catalytic activity and selectivity of high entropy alloy (HEA) towards CO₂ electroreduction was established through first-principles based density functional theory (DFT) by comparing it with pristine Cu (111) surface. This is attributed to the reversal in adsorption trends for two out of the total eight intermediates - *OCH₃ and *O on Cu(111) and HEA surfaces.

Proficient conversion of CO₂ into carbon fuels via electrocatalytic reduction of carbon dioxide (CO₂) can play a key role in sustaining global energy demands¹⁻³. However, this practical applications of the CO₂ reduction reaction (CO₂RR) are currently challenged by the low activity and selectivity due to the high kinetic barriers and competition with the hydrogen evolution reactions in aqueous media⁴⁻⁵. There are several efforts to develop advanced catalysts with specific electronic structures, which could facilitate the CO₂ activation process with high selectivity⁶⁻⁸. Conceptually, tuning the surface area and morphology of the catalysts is extremely important⁹. The nanoparticles demonstrate improved catalytic activities with decent chemical transformation as compared to its bulk counterpart⁹.

The noble-metal catalysts such as Au, Ag, Pt, Pd, have been demonstrated to convert CO₂ to carbon monoxide with high selectivity¹⁰⁻¹⁴. Platinum (Pt), generally considered as the active electrocatalyst for all the electrochemical reactions, generates H₂ exclusively instead of CO₂ reduction in the aqueous medium. Additionally, it is easily poisoned by CO⁵. Recently, copper (Cu) has gained more attention and focus because of its ability to convert CO₂ into higher hydrocarbon fuels¹⁵⁻¹⁸. However, copper-based materials show limited selectivity due to significant hydrogen generation. Interestingly, the bimetallic alloys of this element show an improvement in catalytic activity and selectivity however, CO and H₂ forms in most of the cases with high faradaic efficiency.¹⁹⁻²² The nanomaterials catalysts with substitution of few atoms shows selective conversion of CO₂ to carbon fuel²³. Recently, high entropy alloys (HEAs), a simple solid solution phase, have been studied as multifunctional materials by tuning their thermal, electrical, magnetic and catalytic properties.²⁴⁻²⁷ Their potential applications in electrocatalysis of oxygen reduction reaction²⁵, methanol²⁶, and hydrogen evolution reaction²⁷ have been reported. These multicomponent “cocktails” with simple crystal structure (FCC, BCC or HCP) can effectively be utilized for various functional applications, notably catalytic applications as their composition and constituents can be tuned

for specific applications. This can be done by preparing HEA containing catalytically active metals. Such kind of approach opens new area of single atom catalysts^{9,28}. These HEAs are in general highly active and used without any support but it is possible to disperse them on a support to increase the activity further utilizing the phenomenon of metal support interaction.²⁹⁻³⁰

Here, a unique catalyst based on combination of five active metals (Au, Ag, Pt, Pd and Cu) high entropy alloy has been developed as a ‘single atom catalyst’ in which the Cu atoms are stabilized by other metals in a ‘FCC-facet’ crystalline structures (Figure 1a). A theoretical approach to finding the optimum composition using machine learning is described in detail in Part I: Theoretical Discovery of the present publication. The synergistic impact on Cu with all other metals plays a key role in enhancing stability. HEA also acts as ‘single atom electrocatalysis’ for CO₂RR in an aqueous electrolyte. HEA is utilized as the working electrode, Pt wire as the counter electrode and CO₂ saturated K₂SO₄ as an electrolyte. Gaseous products generated during the electrochemical investigations are analyzed using gas chromatograph. To rationalize the high activity of HEAs from atomistic level, ab-initio density functional theory (DFT) calculations have been performed. It establishes the superior catalytic activity of HEAs, compared to the pristine Cu, based on the thermodynamics study.

The HEA alloy has been synthesized using an easily scalable and precise composition control route of melting and cryogrinding³¹. The XRD pattern of synthesized HEA nanoparticles reveals formation of a single-phase with face-centered cubic structure (FCC) having lattice parameter 0.3936 nm as shown in Figure 1b. Similarly, the nanocrystalline FCC structure was proven by electron diffraction ring pattern. These nanoparticles show average size of 16±10 nm as shown in Figure 1c. The HR-STEM image shown in Figure 1d reveals 001 lattice arrangements with different intensity of individual lattice, which can be assigned to different atoms. All elements (Au, Ag, Pd, Pt, and Cu) were homogeneously distributed or alloyed in

single phase FCC matrix, which is proven by atom probe tomography (APT) as shown in Figure 1e, indicating homogeneous distribution of elements at atomic level. The HEA contains five elements. Therefore, interatomic effects (atoms surrounding) as well as surface oxidation of nanoparticles were revealed using X-ray photoelectron spectroscopy. The elemental peak binding energy has been corrected with adventitious carbon C1s 284.6 eV³². The XPS spectra of the HEAs are shown in Figure 1f. The Pt(4f) core level shows two peaks at 71.1 (Pt4f_{7/2}) and 74.4 (Pt4f_{5/2}) eV similar to bulk Pt³³. Au(4f) core level spectra show two peaks at 84.0 eV and 88.0 eV related to Au(4f_{7/2}) and Au(4f_{5/2}) respectively. This is again similar to bulk Au. Similarly, the binding energy (B.E.) of Pd and Cu confirms the pure metallic characteristic with binding energies similar to their bulk counterpart. Small amount of Cu²⁺ is also observed in the XPS. B.E. for Ag3d_{5/2} which appears at 367.8 eV, 0.4 eV lower than metallic Ag. Clearly, there is some intrinsic charge transfer between Ag and Cu. This phenomenon is consistent with the XPS of bimetallic Au-Ag alloy as well³⁴. The XPS is surface sensitive technique which gives information from few atomic layers (in depth) and Figure 1f confirmed that the AuAgPtPdCu is chemically homogeneous high entropy alloy at the surfaces of nanoparticles, which is the key for catalytic activities of NPs. Similarly, XRD and APT also proved crystal structure and overall composition respectively.

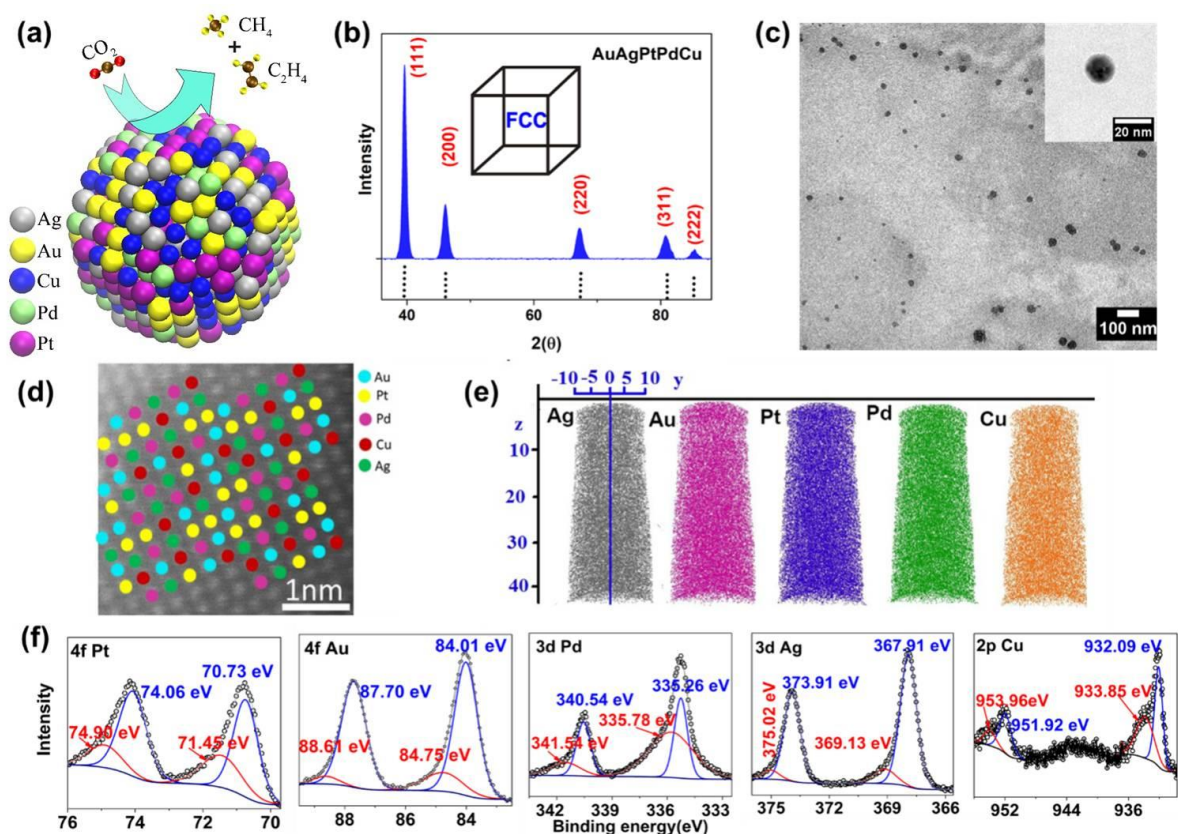


Figure 1: (a) Schematic of the catalysis reaction demonstrated in current work, (b) X-ray diffraction pattern of HEA alloy NPs (AuAgPtPdCu nanoparticles), (c) TEM bright field image of HEA nanoparticles, inset shows high magnification image of single particle. (d) HR-STEM image revealing lattice with color showing different relative intensity marked with color. (e) chemical homogeneity of Au, Ag, Pt, Pd and Cu (mapping of an atom probe microscope) (f) binding energy spectra of HEA nanoparticles (X-ray photoelectron spectroscopy).

Cyclic voltammetry (CV) behavior of HEA coated glassy carbon at 40 mV s^{-1} in $0.5 \text{ M K}_2\text{SO}_4$ is shown in Figure 2. The observed CV showed a prominent redox peak (A1/C1) at -0.13 and -0.32 V (Figure 2a) corresponding to $\text{Cu}^{2+}/\text{Cu}^0$ redox reaction²⁰. Apart from the redox peak (A1/C1), the oxidation and reduction peaks at 0.42 (A2) and 0.25 V (C2) also appear, typical of Pt and Au metal behavior³⁵⁻³⁶. Once the potential range is restricted to the negative side (0.0 to -1.0 V), the peak A1 becomes broad and appear with a shoulder. Corresponding reduction peak (C1) does not appear in this potential range confirming the incomplete surface oxidation. Presence of the redox peak related to $\text{Cu}^{2+}/\text{Cu}^0$ proves that this

species can play a critical role in the catalytic activity. Therefore, the electro-reduction of CO₂ is selected as copper is the most active catalyst for this reaction^{4,15,19-20}.

Figure 2b represents linear sweep voltammetric (LSV) responses of HEA coated glassy carbon electrode containing N₂ (as blank) or CO₂ saturated (purging for 30 min) K₂SO₄ electrolyte. The considerable activity of HEA in CO₂ saturated solution is apparent. Experiments are carried out at 20 mV s⁻¹ in the potential range of 0.0 to -1.0 V vs. Ag/AgCl. The CO₂ reduction starts above -0.5 V, where current density raises rapidly up to -0.8 V and then decreases forming a peak at -0.8V. At -0.8V, the cathodic current density is 10.15 mAcm⁻², ~5 times higher than the N₂ saturated solution (2.2 mAcm⁻²). These observations confirm the significant activity of HEA for CO₂ electroreduction. The corresponding current efficiency (CE %) for electroreduction of CO₂ at different potentials are calculated using equation S1. The highest current efficiency (81.8%) is achieved at -0.8 V (inset of Figure 2b). It is interesting to note that the electrochemical reduction CO₂ is usually carried out in a basic electrolyte such as NaHCO₃. However, in the case of HEA, CO₂ saturated NaHCO₃ (0.5 M) did not yield any activity (Supporting Figure S1(a)). Presently, the reason is unknown, but one can speculate the pH-dependent activity of HEA.

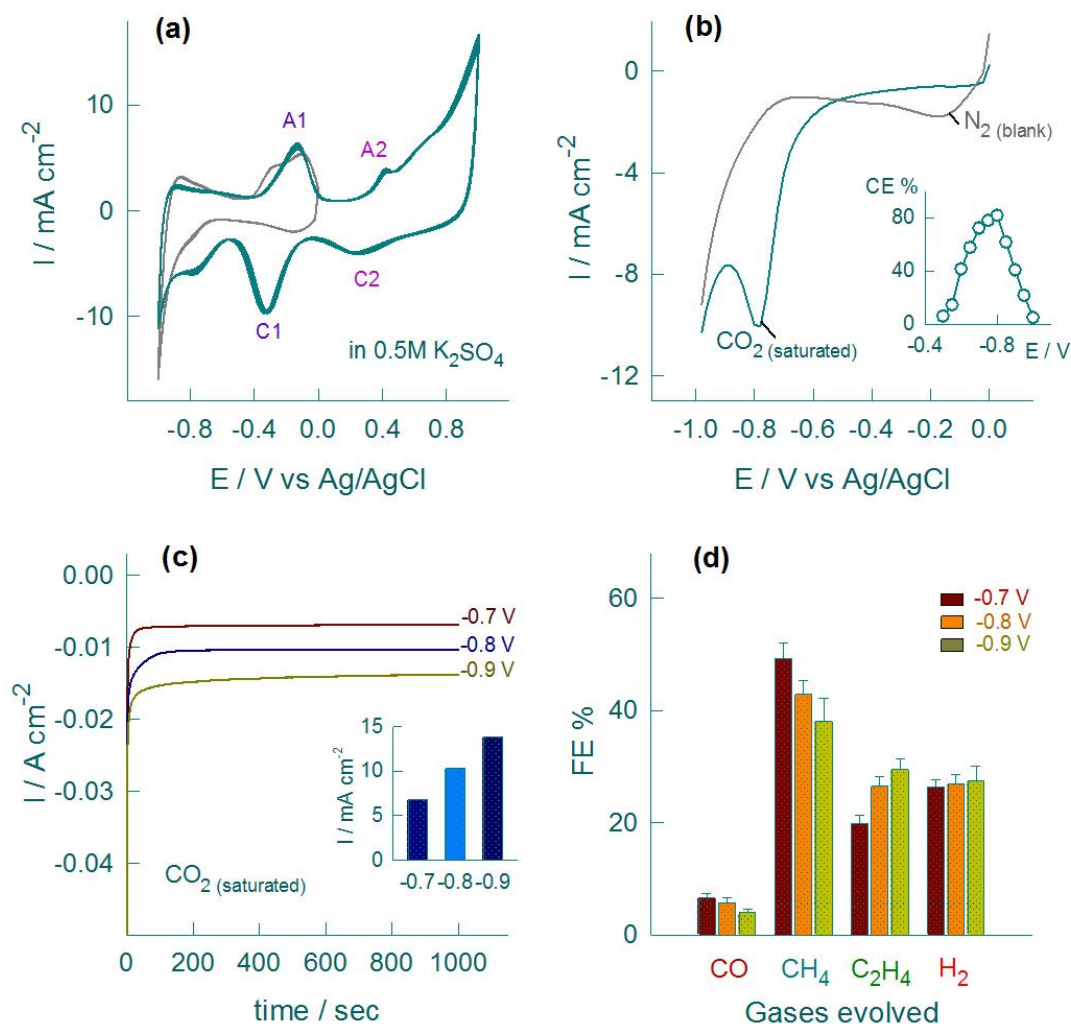


Figure 2: Cyclic voltammetric responses of high entropy alloy catalyst deposited on glassy carbon electrode in blank 0.5 M K_2SO_4 at a scan rate of 40 mV s^{-1} (a), Linear sweep voltammetric response for CO_2RR (saturated for 30 mins) at a scan rate of 20 mV s^{-1} with N_2 purged electrolyte and inset is the plot of current efficiency (CE%) vs. potential (b), Comparative chronoamperometric responses in CO_2 saturated electrolyte at different potentials (-0.7, -0.8 and -0.9 V) for 1000 seconds with respective current density as inset (c). Bar diagram (with errors) for the faradaic efficiencies of their respective carbonaceous species and hydrogen gaseous products (d).

Steady-state current responses of HEA in CO_2 saturated electrolyte at a various potential (-0.7, -0.8 and -0.9V) is also shown in Figure 2c. Obtained steady state current densities are -6.83 mA cm^{-2} (at -0.7V), $-10.31 \text{ mA cm}^{-2}$ (at -0.8V) and $-13.81 \text{ mA cm}^{-2}$ (at -0.9 V), respectively. A bar diagram indicating the impressive CO_2 electroreduction activity of HEA at -0.9 V, is shown in the inset of Figure 2c. The major gaseous products on HEA are CO,

CH₄, C₂H₄ and H₂, similar to the copper-based electrocatalysts³⁷. It is worth noticing that in spite of many elements present in the catalyst, the catalytic effect is depicted only by the copper confirming that other elements are only providing the synergistic effect. Faradaic efficiencies (FE %), calculated as per the equation (S2), are shown in Figure 2d. FE % of CO was ~7 %, at -0.7 V which decreased to 4.0% at -0.9 V. Comparatively, the formation of CH₄ and C₂H₄ was predominantly occurred with FE % up to 49.4% and 19.9 % (at -0.7V), 42.9 % and 26.6 % (at -0.8 V) and 38.0% and 29.5% (at -0.9 V), respectively. The FE % for hydrogen on HEA catalyst is about 26.4% which does not change significantly at other potentials. Importantly, the total faradaic efficiency is 100 % for the gaseous products combined at the lowest applied potential, i.e., -0.9 V vs. Ag/AgCl (-0.3 V vs. reversible hydrogen electrode). This confirms that there is zero or negligible liquid product formation highlighting the unique capability of HEA catalyst. A detailed catalytic activity comparison of HEA with other reported catalysts is given in Table S1 (in supporting information). One can notice that HEA performs the best in terms of low applied voltage and striking hydrocarbon efficiency. Long term stability of HEA is studied using chronoamperometry for 5 hours in K₂SO₄ solution (Figure S1(b)). Electrolyte is continuously bubbled with CO₂ during the experiment. Initially, current decreases reaching a steady state, which remains constant for 5 hours. This highlights the stability of HEA.

To gain an insight into the reaction, we have performed DFT calculations. We compared the catalytic activity of the multicomponent HEA with Cu to bring about the salient features of the HEA as catalysts for CO₂RR. The aim is to provide the mechanisms for excellent catalytic activity of HEA. The optimized lattice parameters of Cu are found to be, $a = b = c = 3.63 \text{ \AA}$ (Figure S2a), which is in excellent agreement with the previous reports³⁸. The (111) facet was chosen for calculations, as it is the most stable facet of the FCC metals. The supercell size of the Cu (111) surface was selected as 5x3x1 to get all the possible adsorbing

sites, which are also present in the HEAs (Figure S2 and S3(a)). The unit cell of HEAs contained 120 atoms, with the constituent elements - Pt, Pd, Ag, Au and Cu, being equal in proportion (20 % each). The method for generation of the structure of HEA utilized in the present study is described in detail in the supporting information file. Based on experimental composition, the Au:Ag:Pt:Pd:Cu=1:1:1:1:1 composition was chosen for simulations. Then quantification of the catalytic activity of pristine Cu was performed using the scheme provided by Norskov *et al.*³⁹⁻⁴⁰ For this purpose, the adsorption energies of all the intermediates involved in the eight-step CO₂RR (equations S1-S8) was calculated from DFT using the expressions given in supplementary information (equations S9-S15). Subsequently, these intermediate adsorption energies were converted into Gibb's free energies of adsorption^{39,41} using:

$$\Delta G_{inter}^{ads} = \Delta E_{inter}^{ads} + \Delta ZPE - T\Delta S - \Delta G_U \quad (1)$$

where ΔZPE is the difference in zero-point energies, ΔS is the change in entropy due to vibrational contributions, and $\Delta G_U = -eU$, where U is the applied electrode potential. The values of zero-point energies and entropies for the intermediates and reference molecules have been taken from the reported literature³⁹. The complete free-energy reaction profile for CO₂RR is given in Figure S5. The reaction profile at 0 V is shown by black curves, where three elementary steps are endoergic, i.e., *CO to *CHO, *OCH₃ to *O, and the final step involves the release of a water molecule from *OH intermediate. Out of these three, the elementary step for the conversion of OCH₃ into O intermediate has the highest barrier of 1.91 eV and is, therefore, the rate-determining step (RDS) for CO₂RR on Cu (111) surface. This barrier is also the theoretical limiting potential for the reduction reaction on pristine Cu surface, as at $U = -1.91$ V, all the elementary steps become exoergic. We then extended this thermodynamic study to the HEA system. In this case, there is a possibility of a large number of catalytic centers due to the five elements being present randomly on the surface. In order

to mitigate this problem, we chose only one catalytic center from electronic principles of designing catalyst, i.e., based on position of d-band center (E_{dBC}). In general, the activity of any catalytic reaction is related to the d-band center of the metal under consideration⁴². Therefore, d-band centers of all the atoms present on the topmost layer of the HEA slab (Figure S3(a)) have been plotted in both the up and down spin configurations in Figure S6. From this plot, we notice that Pd¹¹ atom has the value of E_{dBC} closest to the Fermi level (E_F) in both spin configurations. Hence it was chosen as the catalytic center for CO₂RR study. Pd¹¹ is also adjacent to a Cu atom on the surface (Cu⁷; Figure S3(a)), which would enhance the catalytic activity of Pd¹¹ center. The free-energy profile for the HEA system is shown in Figure 3. The two endoergic reactions, which are same as in the case of pristine Cu (111) surface are *CO to *CHO, and *OCH₃ to *O conversions.

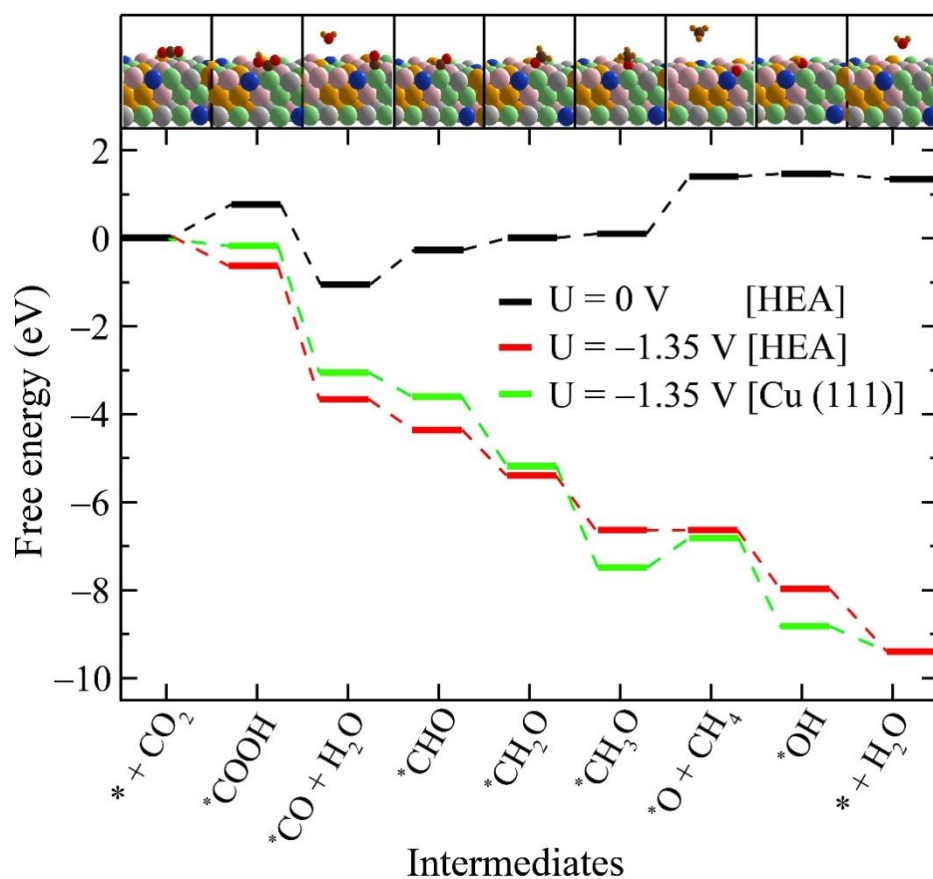


Figure 3: Free energy diagram of CO₂RR on AuAgPtPdCu HEA surface. Optimized structures of all the intermediates on HEA surface are shown in the inset. Grey, green, pink,

yellow, blue, brown, red and orange spheres represent Pt, Pd, Ag, Au, Cu, C, O, and H atoms, respectively.

However, the barriers in this system are reduced significantly, e.g., 0.73 eV for the 3rd elementary step and 1.35 eV for the 6th elementary step. Hence, at a potential of -1.35 V, the reaction profile becomes downhill in energy. The free energy profile of Cu (111) surface is also plotted at the same potential in Figure 3, which is depicted by green lines. It is clear that at this potential, the step of *OCH_3 to *O conversion is still uphill, requiring more external potential to overcome this barrier. Therefore, the theoretical limiting potential for HEA system is lower than that of pristine Cu metal, implying the thermodynamic favoring of CO_2RR on the HEA surface over the Cu (111) surface. This is in agreement with the experimental observations. The reduced theoretical limiting potential for HEA system can be attributed to the destabilization of *OCH_3 intermediate and stabilization of the *O intermediate on the HEA surface, compared to the Cu (111) surface. The extra stabilization of *O intermediate on the HEA surface may be because both Pd^{11} and Cu^7 atoms are bonded to the O atom. This behavior can be explained from the partial density of states (PDOS) plotted in Figures S7 and S8 for *OCH_3 and *O intermediates, respectively. While in the case of *OCH_3 intermediate on Cu (111) surface, the hybridized states of O and Cu^{96} atom are filled and more broadened while all hybridized states of O and Pd^{11} are sharply peaked. Moreover, one state in down spin configuration is unfilled on HEA surface. This would lead to stronger binding of OCH_3 on the Cu (111) surface. Cu^{96} and Pd^{11} are the sites through which OCH_3 intermediate gets adsorbed on the two surfaces under consideration. Similarly, the states of O intermediate on Cu (111) are sharply peaked, while those on the HEA surface are broader, resulting in better adsorption of O intermediate on HEA than on the Cu (111) surface. In this

case, O adsorbs through 3 atoms (hcp type of adsorption site) – Cu⁸⁸, Cu⁹⁶, and Cu¹⁰⁸ atoms on pristine Cu slab, and Cu⁷, Cu¹², and Pd¹¹ atoms on the HEA slab.

To confirm whether the CO₂RR activity on HEA follows the trend in d-band center, we carried out same free energy calculations on the Cu⁷ active site also (Figure S9). In this case, two steps have almost similar barriers (*COOH to *CO and *OCH₃ to *O), however, the *OCH₃ to *O step has slightly higher barrier (1.54 eV), leading to a limiting potential of -1.54 V. Therefore, Cu⁷ is less active than Pd¹¹ site on account of its lower limiting potential (limiting potential of Pd¹¹ = -1.35 V). This trend is, therefore, in agreement with the trend in their respective d-band centers⁴². Further, to understand the selectivity of different products observed in the experiments (Table S1), we calculated free energy diagrams for CO (Figure S10) and H₂ (Figure S11) evolution reactions on Pd¹¹ site of HEA. Although, limiting potential for CO evolution is higher than that of CH₄ formation, however, free energy adsorption of CO is -1.01 eV, which is highly exothermic. This makes CO difficult to be desorbed from the surface of HEA, and hence experimental Faradaic efficiency for CO is very low (4.9%). Moreover, free energy adsorption of H₂ is -0.45 eV, while for efficient HER catalysts, this value is usually thermoneutral, i.e., $|\Delta G_{\text{ads}}(\text{H})| \approx 0$ ⁴¹. Hence, Au-Ag-Pt-Pd-Cu HEA is selective for hydrocarbon products rather than hydrogen in agreement with the trend in experimental Faradaic efficiency, which is lower for H₂ than that of CH₄ and C₂H₄ (Table S1).

In conclusion, we demonstrated that the unprecedented catalytic activity of cryomilled prepared nanocrystalline equiatomic Au-Ag-Pt-Pd-Cu high entropy alloy for efficient electrochemical reduction of CO₂RR. The optimum composition may be found using the approach described in Part I of the manuscript. Collective characterizations such as XRD, HRTEM, and XPS reveal the atomic distribution in the HEA. In spite of many elements present in the catalyst, the electrocatalytic activity is predominantly described by the presence

of redox active Cu metal ($\text{Cu}^{2+}/\text{Cu}^0$), and other metals only provide a synergistic effect. Complete 100% conversion of CO_2 to gaseous products at lower potential (-0.3 V RHE) highlights the uniqueness HEA and making it different from Cu metal alone. The density functional theory (DFT) studies establish the HEAs as a superior catalyst, compared to the pristine Cu metal, based on the free energy calculations of intermediates.

ASSOCIATED CONTENT

The Supporting Information is available free of charge on the ACS Publications websites. Detailed synthesis procedure, experimental and instrumentation details, computational DFT studies and calculations (PDF).

AUTHOR INFORMATION

**Corresponding Authors*

E-mail: ssharma@iitgn.ac.in (S.S*), abhishek@iisc.ac.in (A.K.S*),
Chandra.tiwary@metal.iitkgp.ac.in (C.S.T*), kbiswas@iitk.ac.in (K.B*)

Notes

The authors declare no competing financial interest.

ACKNOWLEDGMENTS

S.S. and S.N. acknowledges DST-SERB (EMR/2016/000806) project for the funding and fellowship. A.P, R.K. and A.K.S. acknowledge Materials Research Centre, Solid State and Structural Chemistry Unit, and Supercomputer Education and Research Centre for providing the computational facilities. A.P, R.K. and A.K.S. also acknowledge the support from Institute of Eminence (IoE) MHRD grant of Indian Institute of Science.

AUTHOR CONTRIBUTIONS

K.B, S.S. A.K.S. and C.S.T. envisaged the idea and executed the experiments. N.K.K. synthesized and characterized the HEA material. S.N. carried out electrocatalysis. R.K. and

A.P carried out DFT calculations. K.D.M. and K.G.P. performed the transmission microscopy experiments. All the authors contributed to the data analysis and writing and gave approval for the final submission.

REFERENCES

- (1) Costentin, C.; Roberta, M.; Saveant, J.M. Catalysis of the Electrochemical Reduction of Carbon dioxide. *Chem. Soc. Rev.* **2013**,*42*, 2423-2436.
- (2) Qiao, J.; Liu, Y.; Hong, F.; Zhang, J. A Review of Catalysts for the Electroreduction of Carbon Dioxide to Produce Low-Carbon Fuels. *Chem. Soc. Rev.* **2014**,*43*, 631-675.
- (3) Liu, C.; Colon, B. C.; Ziesack, M.; Silver, P. A.; Nocera, D. G. Water Splitting–Biosynthetic System with CO₂ Reduction Efficiencies Exceeding Photosynthesis. *Science* **2016**,*352*, 1210–1213.
- (4) Li, C. W.; Ciston, J.; Kanan, M. W. Electroreduction of Carbon Monoxide to Liquid Fuel on Oxide-Derived Nanocrystalline Copper. *Nature* **2014**,*508*, 504-507.
- (5) Kuhl, K. P.; Hatsukade, T.; Cave, E. R.; Abram, D. N.; Kibsgaard, J.; Jaramillo, T. F. Electrocatalytic Conversion of Carbon Dioxide to Methane and Methanol on Transition Metal Surfaces. *J. Am. Chem. Soc.* **2014**,*136*, 14107–14113.
- (6) Cheng, Y.; Zhao, S.; Johannessen, B.; Veder, J.-P.; Saunders, M.; Rowles, M. R.; Cheng, M.; Liu, C.; Chisholm, M. F.; Marco, R. D.; Cheng, H.-M.; Yang, S.-Z.; Jiang, S. P. Atomically Dispersed Transition Metals on Carbon Nanotubes with UltraHigh Loading for Selective Electrochemical Carbon Dioxide Reduction. *Adv. Mater.* **2018**,*30*, 1706287-1706293.
- (7) Mori, K.; Taga, T.; Yamashita, H. Isolated Single-Atomic Ru Catalyst Bound on a Layered Double Hydroxide for Hydrogenation of CO₂ to Formic Acid. *ACS Catal.* **2017**,*7*, 3147–3151.
- (8) Back, S.; Lim, J.; Kim, N.Y.; Kim, Y.-H.; Jung, Y. Single-Atom Catalysts for CO₂ Electroreduction with Significant Activity and Selectivity Improvements. *Chem. Sci.* **2017**,*8*, 1090-1096.
- (9) Wang, A.; Li, J.; Zhang, T. Heterogeneous Single-Atom Catalysis. *Nat. Rev. Chem.* **2018**,*2* (6), 65-81.
- (10) Zhu, W.; Michalsky, R.; Metin, O.; Lv, H.; Guo, S.; Wright, C. J.; Sun, X.; Peterson, A. A.; Sun, S. Monodisperse Au Nanoparticles for Selective Electrocatalytic Reduction of CO₂ to CO. *J. Am. Chem. Soc.* **2013**,*135*, 16833- 16836.

- (11) Ma, M.; Trzeźniewski, B. J.; Xie, J.; Smith, W. A. Selective and Efficient Reduction of Carbon Dioxide to Carbon Monoxide on Oxide-Derived Nanostructured Silver Electrocatalysts. *Angew. Chem. Int. Ed.* **2016**, *55* (33), 9748-9752.
- (12) Mistry, H.; Reske, R.; Zeng, Z.; Zhao, Z. J.; Greeley, J.; Strasser, P.; Cuenya, B. R. Exceptional Size-Dependent Activity Enhancement in the Electroreduction of CO₂ over Au Nanoparticles. *J. Am. Chem. Soc.* **2014**, *136*, 16473-16476.
- (13) Gao, D.; Zhou, H.; Wang, J.; Miao, S.; Yang, F.; Wang, G.; Wang, J.; Bao, X. Size-Dependent Electrocatalytic Reduction of CO₂ over Pd Nanoparticles. *J. Am. Chem. Soc.* **2015**, *137*, 4288-4291.
- (14) Kim, C.; Jeon, H. S.; Eom, T.; Jee, M. S.; Kim, H.; Friend, C. M.; Min, B. K.; Hwang, Y. J. Achieving Selective and Efficient Electrocatalytic Activity for CO₂ Reduction Using Immobilized Silver Nanoparticles. *J. Am. Chem. Soc.* **2015**, *137*, 13844–13850.
- (15) Manthiram, K.; Beberwyck, B. J.; Alivisatos, A. P. Enhanced Electrochemical Methanation of Carbon Dioxide with a Dispersible Nanoscale Copper Catalyst. *J. Am. Chem. Soc.* **2014**, *136*, 13319–13325.
- (16) Reske, R.; Mistry, H.; Behafarid, F.; Cuenya, B. R.; Strasser, P. Particle Size Effects in the Catalytic Electroreduction of CO₂ on Cu Nanoparticles. *J. Am. Chem. Soc.* **2014**, *136*, 6978-6989.
- (17) Xie, J.-F.; Huang, Y.-X.; Li, W.-W.; Song, X.-N.; Xiong, L.; Y, H.-Q. Efficient Electrochemical CO₂ Reduction on a Unique Chrysanthemum-Like Cu Nanoflower Electrode and Direct Observation of Carbon Deposit. *Electrochim. Acta* **2014**, *139*, 137-144.
- (18) Raciti, D.; Livi, K. J.; Wang, C. Highly Dense Cu Nanowires for Low-Overpotential CO₂ Reduction. *Nano Lett.* **2015**, *15*, 6829–6835.
- (19) Kim, D.; Resasco, J.; Yu, Y.; Asiri, A. M.; Yang, P. Synergistic Geometric and Electronic Effects for Electrochemical Reduction of Carbon Dioxide Using Gold–Copper Bimetallic Nanoparticles. *Nat. Commun.* **2014**, *5*, 4948-4956.
- (20) Li, Q.; Fu, J.; Zhu, W.; Chen, Z.; Shen, B.; Wu, L.; Xi, Z.; Wang, T.; Lu, G.; Zhu, J.-j.; Sun, S. Tuning Sn-Catalysis for Electrochemical Reduction of CO₂ to CO via the Core/Shell Cu/SnO₂ Structure. *J. Am. Chem. Soc.* **2017**, *139*, 4290-4293.
- (21) Ma, S.; Sadakiyo, M.; Heima, M.; Luo, R.; Haasch, R. T.; Gold, J. I.; Yamauchi, M.; Kenis, P. J. A. Electroreduction of Carbon Dioxide to Hydrocarbons Using Bimetallic Cu–Pd Catalysts with Different Mixing Patterns. *J. Am. Chem. Soc.* **2017**, *139*, 47-50.

- (22) Liu, K.; Ma, M.; Wu, L.; Valenti, M.; Cardenas-Morcoso, D.; Hofmann, J. P.; Bisquert, J.; Gimenez, S.; Smith, W. A. Electronic Effects Determine the Selectivity of Planar Au–Cu Bimetallic Thin Films for Electrochemical CO₂ Reduction. *ACS Appl. Mater. Interfaces* **2019**,*11*, 16546–16555.
- (23) Zhou, S.; Varughese, B.; Eichhorn, B.; Jackson, G.; McIlwrath, K. Pt–Cu Core–Shell and Alloy Nanoparticles for Heterogeneous NO_x Reduction: Anomalous Stability and Reactivity of a Core–Shell Nanostructure. *Angew. Chem. Int. Ed.* **2005**,*44* (29), 4539-4543.
- (24) Ye, Y.F.; Wang, Q.; Lu, J.; Liu, C.T.; Yang, Y. High-Entropy Alloy: Challenges and Prospects. *Materials Today* **2016**,*19* (6), 349-362.
- (25) Löffler, T.; Meyer, H.; Savan, A.; Wilde, P.; Manjón, A. G.; Chen, Y.-T.; Ventosa, E.; Scheu, C.; Ludwig, A.; Schuhmann, W. Discovery of a Multinary Noble Metal–Free Oxygen Reduction Catalyst. *Adv. Energy Mater.* **2018**,*8* (34), 1802269-1802276.
- (26) Wang, A.-L.; Wan, H.-C.; Xu, H.; Ye-Xiang; Li, T. G.-R. Quinary PdNiCoCuFe Alloy Nanotube Arrays as Efficient Electrocatalysts for Methanol Oxidation. *Electrochim. Acta* **2014**,*127*, 448-453.
- (27) Zhang, G.; Ming, K.; Kang, J.; Huang, Q.; Zhang, Z.; Zheng, X.; Bi, X. High Entropy Alloy as a Highly Active and Stable Electrocatalyst for Hydrogen Evolution Reaction. *Electrochim. Acta* **2018**,*279*, 19-23.
- (28) Qiao, B.; Wang, A.; Yang, X.; Allard, L. F.; Jiang, Z.; Cui, Y.; Liu, J.; Li, J.; Zhang, T. Single-atom Catalysis of CO Oxidation Using Pt₁/FeO_x. *Nature Chem.* **2011**,*3*, 634-641.
- (29) Kumari, N.; Sinha, N.; Haider, M. A.; Basu, S. CO₂ Reduction to Methanol on CeO₂ (110) Surface: A Density Functional Theory Study. *Electrochim. Acta* **2015**,*177*, 21-29.
- (30) Kumari, N.; Haider, M. A.; Agarwal, M.; Sinha, N.; Basu, S. Role of Reduced CeO₂ (110) Surface for CO₂ Reduction to CO and Methanol. *J. Phys. Chem. C* **2016**,*120*, 16626–16635.
- (31) Kumar, N.; Tiwary, C. S.; Biswas, K. Preparation of Nanocrystalline High-Entropy Alloys via Cryomilling of Cast Ingots. *J. Mater. Sci.* **2018**,*53*, 13411-13423.
- (32) Yu, X.; Hantsche, H. Some Aspects of the Charging Effect in Monochromatized Focused XPS. *Fresenius J. Anal. Chem.* **1993**,*346* (1), 233-236.
- (33) Shyu, J. Z.; Otto, K. Identification of Platinum Phases on γ -alumina by XPS. *Appl. Surf. Sci.* **1988**,*32* (1), 246-252.

- (34) Wang, A.-Q.; Liu, J.-H.; Lin, S. D.; Lin, T.-S.; Mou, C.-Y. A Novel Efficient Au–Ag Alloy Catalyst System: Preparation, Activity, and Characterization. *J. Catal.* **2005**,*233* (1), 186-197.
- (35) Ge, X.; Wang, R.; Liu, P.; Ding, Y. Platinum-Decorated Nanoporous Gold Leaf for Methanol Electrooxidation. *Chem. Mater.* **2007**,*19*, 5927-5829.
- (36) Ballarin, B.; Gazzano, M.; Scavetta, E.; Tonell, D. One-Step Electrosynthesis of Bimetallic Au-Pt Nanoparticles on Indium Tin Oxide Electrodes: Effect of the Deposition Parameters. *J. Phys. Chem. C* **2009**,*113*, 15148-15154.
- (37) Hori, Y.; Murata, A.; Takahashi, R. Formation of Hydrocarbons in the Electrochemical Reduction of Carbon Dioxide at a Copper Electrode in Aqueous Solution. *J. Chem. Soc., Faraday Trans. 1*, **1989**,*85* (8), 2309-2326.
- (38) Straumanis, M. E.; Yu, L. S. Lattice Parameters, Densities, Expansion Coefficients and Perfection of Structure of Cu and of Cu-In α Phase. *Acta Cryst.*, **1969**,*A25*, 676-682.
- (39) Peterson, A. A.; Abild-Pedersen, F.; Studt, F.; Rossmeisla, J.; Nørskov, J. K. How Copper Catalyzes the Electroreduction of Carbon Dioxide into Hydrocarbon Fuels. *Energy Environ. Sci.* **2010**,*3*, 1311-1315.
- (40) Peterson, A. A.; Nørskov, J. K. Activity Descriptors for CO₂ Electroreduction to Methane on Transition-Metal Catalysts. *J. Phys. Chem. Lett.* **2012**,*3*, 251–258.
- (41) Kumar, R.; Das, D.; Singh, A. K. C₂N/WS₂ Van der Waals type-II Heterostructure as a Promising Water Splitting Photocatalyst. *J. Catal.* **2018**,*359*, 143-150.
- (42) Nørskov, J. K.; Abild-Pedersen, F.; Studt, F.; Bligaard, T. Density Functional Theory in Surface Chemistry and Catalysis. *Proc. Natl. Acad. Sci.* **2011**,*108*, 937-943.

TOC

